IEEE Access
Multidisciplinary ⋮ Rapid Review ⋮ Open Access Journal

Received November 13, 2020, accepted January 8, 2021, date of publication February 2, 2021, date of current version February 9, 2021.

Digital Object Identifier 10.1109/ACCESS.2021.3056464

Efficient Filter Generation Based on Particle Swarm Optimization Algorithm

LIANG ZENG[1], JINTAI LI[2,3,4], JIANXIN LIU[2,3,4], RONGWEN GUO[2,3,4], HANG CHEN[2,3,4], AND RONG LIU[2,3,4]

[1]School of Mathematical Sciences, Xiamen University, Xiamen 361005, China
[2]School of Geosciences and Info-Physics, Central South University, Changsha 410083, China
[3]Laboratory of Non-ferrous Resources and Geological Hazard Detection, Central South University, Changsha 410083, China
[4]Key Laboratory of Metallogenic Prediction of Nonferrous Metals, Ministry of Education, Central South University, Changsha 410083, China

Corresponding author: Rong Liu (liurongkaoyan@126.com)

This work was supported by the National Natural Science Foundation of China under Grant 41904158, Grant 42004065, and Grant 42074165.

ABSTRACT The evaluation of Hankel integration is an important part in the interpretation of electromagnetic (EM) data, especially in physical and geophysical applications. The digital linear filter (DLF) method is commonly applied. For an optimal digital filter design based on matrix inversion, it requires optimization over the model space of the spacing and shift. This is typically obtained by a grid search algorithm on gradually refined grids. In this paper, we apply a particle swarm algorithm to optimize the spacing and shift in the model space. In this algorithm, we use a group of particles to search the model space and do not have to grid the model space sequentially to finer meshes. It has been applied to search the optimal spacing and shift for analytical function pairs, indicating a fast convergence. The performance of the obtained 201-point filter is examined and compared with other published filters based on analytic function pairs and controlled source electromagnetic (CSEM) applications. The results indicate that the proposed 201-point filters have a good numerical performance in terms of accuracy over a large offset range.

INDEX TERMS Electromagnetics, transforms, digital filters, Hankel transform.

I. INTRODUCTION

The calculation of Hankel integrals is typically required in optics, electromagnetics (EM), and electronic engineering. However, for these practical applications, most Hankel integral problems generally have no analytical solution and can only be calculated numerically. The oscillation characteristic of Bessel functions makes the calculation of numerical integration difficult. Therefore, the calculation of the Hankel integral is considered as one of the most important parts in, for example, numerical modeling of EM responses in geophysical applications [1]–[9],and numerous work has been dedicated to solve this integral [10]–[15].

The digital linear filter method makes the calculation of the Hankel integration more practical [16]. This algorithm transforms the Hankel integral into convolution and calculates the filter spectrum. The filter coefficients can be obtained by the inverse Fourier transform of the spectrum. Later authors work on developing efficient digital filters for solving the Hankel transform of different applications [17]–[23]. The filter coefficients can also be obtained with the direct integration method as proposed by authors, which is less commonly used in the literature [24], [25].

For most applications, since no analytic solutions are available, the accuracy of the filters for one specific problem can be hard to be justified. For this purpose, some authors develop the direct integration method to provide an accurate evaluation of the Hankel transform [26], [27]. Especially after Key [28] made his integration code publicly available, the Hankel transform solution from direct integration is used as a benchmark for other methods, facilitating people to develop more efficient and accurate filters.

More recently authors develop the matrix inversion method to calculate the filters by directly discretizing the Hankel transformation [29], [30]. This can be considered as a variant of the Wiener-Hopf least square method [27], [31]. This method needs to find optimal spacing and shift parameter, which are optimized over a sequence of gradually refined grids. The literature shows that the optimal solution of the spacing and shift parameter can be random over a large

The associate editor coordinating the review of this manuscript and approving it for publication was Su Yan.

detailed region (in this region every filter is good), and the refinement needs expertise especially during the last stages of the search process [30]. Automatic determination of optimal spacing and shift parameters is of practical importance and not reported in the literature, which is the primary goal of this paper.

In this paper, to avoid the gradual refinement process and subjective choice of one particular randomly-distributed solution, we apply the particle swarm algorithm to search an optimal solution (spacing and shift parameters). In Methodology part, we have a brief review of digital linear filter technology and then have a description of particle swarm algorithm. In the Numerical test, the designed filter is compared with other filters developed in the literature based on analytic function pairs and three controlled source electromagnetic (CSEM) applications. Its numerical performance is examined based on the comparison. In the conclusion, we summarized the numerical performance of our algorithm.

II. METHODOLOGY

A. HANKEL TRANSFORM CALCULATION

The Hankel transform of $f(l)$ with the kernel being Bessel function of the first kind is defined as

$$F(r) = \int_0^\infty f(l) J_n(lr)dl, \tag{1}$$

where n typically used in real applications is 0 or 1, and f is the function being transformed. By substituting $r = e^x$ and $l = e^{-y}$, and multiplying by e^x on both sides of (1), we obtain

$$e^x F(e^x) = \int_{-\infty}^\infty f(e^{-y}) J_n(e^{x-y}) e^{x-y} dy, \tag{2}$$

which is a convolution equation. With the discretization of $x = \Delta m$ and $y = \Delta n$ (Δ is the sampling interval or the spacing), equation (2) can be approximated by

$$e^{\Delta m} F(e^{\Delta m}) = \sum_{n=-\infty}^{\infty} f(e^{-\Delta n}) e^{\Delta(m-n)} J_n(e^{\Delta(m-n)}), \tag{3}$$

Equation (3) is a discrete form of the convolution equation. Practically, to produce more accurate integration results, we typically shift y by δ. Then equation (3) can be rewritten as

$$e^{\Delta m} F(e^{\Delta m}) = \sum_{n=-\infty}^{\infty} f(e^{-\Delta n-\delta}) e^{\Delta(m-n-\delta)} J_n(e^{\Delta(m-n-\delta)}), \tag{4}$$

in the standard convolution form, equation (4) can be written as

$$g(m) = \sum_{n=-\infty}^{\infty} f(n) h_n(m-n) = \sum_{n=-\infty}^{\infty} f(m-n) h_n(n) \tag{5}$$

where $g(m) = e^{\Delta m} F(e^{\Delta m})$, taken as the output of the linear system, $f(m-n) = f(e^{-\Delta(m-n-\delta)})$ is considered as the input function, and h_n is the unknown kernel response function (filter coefficients). For a filter with limited number of points (e.g., N), then (1) at any offset r_m can be evaluated as

$$F(r_m) = \sum_{n=1}^{N} \frac{f(\frac{e^{\Delta n+\delta}}{r_m}) h_n}{r_m} \tag{6}$$

to solve (6), we need to know h_n. This can be performed in both the spectrum and sample domains based on analytical Hankel transform pairs (with known inputs and outputs). For example, in this paper we use the following analytical Hankel transform pairs (also used in the literature [19]), given by

$$\int_0^\infty l exp(-al^2) J_0(lr)dl = \frac{exp(-\frac{r^2}{4a})}{2a}, \tag{7}$$

$$\int_0^\infty l^2 exp(-al^2) J_1(lr)dl = \frac{r}{4a^2} exp(-\frac{r^2}{4a}), \tag{8}$$

where $a > 0$, $r > 0$.

In the spectrum domain, the convolution of the two functions in (5) can be transformed into simple multiplication and the kernel response spectrum (filter response) can be easily obtained by dividing the output with the input. The filter spectrum is then inverse Fourier transformed to calculate the filter response in the sample domain. In this paper, we directly calculate the kernel response in the sample domain as in Kong [29]. We assume that h_n has a limited length N in the sample domain. From (6), we need N equations at $r_m, m = 1 \ldots N$, to solve the kernel response $h_n, n = 1 \ldots N$, with known input and output (from analytical Hankel transform pairs). Then the calculation of h_n based on (6) is equivalent to solve the following linear system in matrix form as

$$\boldsymbol{g} = \boldsymbol{A}\boldsymbol{h} \tag{9}$$

where $\boldsymbol{g}$ is the vector with elements of $g_m = F(r_m)$, $\boldsymbol{h}$ is the vector with elements of h_n and $\boldsymbol{A}$ is the matrix with entries of $\frac{f(e^{\Delta n+\delta}/r_m)h_n}{r_m}$.

Once $\boldsymbol{h}$ is calculated from (9), then we use (6) to calculate the Hankel integration in (1) for any functions. Previous studies show that the choice of the spacing and shift parameters impacts the filter calculation and influences the accuracy of Hankel transform calculation based on the digital filter method [31]. In order to produce an accurate evaluation of the Hankel integral, we need to obtain the optimal digital filters based on searching over the spacing and shift parameter space [30].

B. PARTICLE SWARM ALGORITHM

The particle swarm algorithm was initially proposed by Eberhart and Kennedy for the optimization of nonlinear continuous functions [32]. Within this algorithm, a group of particles are used and each particle retains its best solution encountered during the optimization process (the best position of an individual). At the same time, the algorithm has memory of the global best position for the particle group. With proper choice, the particle swarm algorithm can converge to the global best solution efficiently.

To better understand the particle swarm methodology, we give a brief introduction on how it works: A group of particles consisting of m individuals (models) in the N-dimensional parameter space are generated with random positions and initial velocities. In each iteration, the movement of a particle is affected by the particle's own historical best position *Pbest* and the historical best position of the particle group *Gbest*. The velocity v_j and position X_j of each particle are updated in the manner as defined by

$$v_j = \omega v_j + c1 \cdot r1_j \cdot (Pbest_j - X_j) + c2 \cdot r2_j \cdot (Gbest - X_j) \tag{10}$$

$$X_j = X_j + v_j \tag{11}$$

where ω is the inertia weight, and $c1$ and $c2$ are the learning factors, which determine the convergence speed of the particles to *Pbest* and *Gbest*; j is the jth individual particle, and $r1_j$ and $r2_j$ are the random weights in the range [0,1] corresponding to each particle generated for each iteration. The second term on the right of (10) makes the particle move to its own historical best position. The third term makes the particle move to the historical best position of the group. During the inversion, ω, $c1$ and $c2$ are decreasing linearly [33].

After calculating the fitness of all individuals for each iteration, the algorithm updates the best positions of both the individual and the particle group as indicated in Fig. 1. Once the optima spacing and shift is obtained, we can calculate the filter response. The Hankel transform for general functions can be calculated using (9).

Algorithm 1 PSO algorithm to optimize parameters

```
Input: Minimization criteria function $f(\mathbf{X})$, domain of $\Delta$ & $\delta$
Output: $\Delta, \delta$
    initialize: $\mathbf{X}^0 \leftarrow$ random points in the domain of $\Delta$ & $\delta$
    initialize: $\mathbf{v}^0 \leftarrow$ random velocity
    $\mathbf{P}_{best} \leftarrow \mathbf{X}^0$
    $G_{best} \leftarrow \mathbf{X}_{best}[argmin(f(\mathbf{P}_{best}))]$
    for $i = 1, 2, ..., T$ do
        if $G_{best}$ does not change for 15 iterations then
            return $\Delta, \delta \leftarrow G_{best}$
        end if
        $\mathbf{v}^i = \omega \mathbf{v}^{i-1} + c1 \cdot \mathbf{r1}^i \cdot (\mathbf{P}_{best} - \mathbf{X}^{i-1}) + c2 \cdot \mathbf{r2}^i \cdot (G_{best} - \mathbf{X}^{i-1})$
        $\mathbf{X}^i = \mathbf{X}^{i-1} + \mathbf{v}^i$
        $updateID \leftarrow isSmaller(f(\mathbf{X}^i), f(\mathbf{P}_{best}))$
        $\mathbf{P}_{best}[updateID] \leftarrow \mathbf{X}^i[updateID]$
        $G_{best} \leftarrow \mathbf{P}_{best}[argmin(f(\mathbf{P}_{best}))]$
    end for
```

FIGURE 1. The flow of particle swarm algorithm.

C. OBJECTIVE FUNCTION

For each iteration as shown in Fig. 1, we update a group of particles P^i. For each particle, it comprises the spacing Δ and shift δ. The following steps are used to calculate the response filters and fitness for $f(x)$ (typically has analytical Hankel transform) for each particle:

1) Calculate $e^{\Delta m}$ (i.e., r_m offset) and $e^{\Delta n+\delta}$ (filter abscissa) at N offsets and N abscissae (chosen by users).
2) Calculate the Hankel transform analytically (e.g., right hand side of (7) or (8)) to form $\boldsymbol{g}$ and $f(e^{\Delta n+\delta}/e^{\Delta m})/e^{\Delta m}$ to form $\boldsymbol{A}$ in (9) and then invert $\boldsymbol{A}$ for $\boldsymbol{h}$.
3) Now using $\boldsymbol{h}$ and the same analytical function pair, we can calculate the numerical solution $F(r_i)$ at any r_i according to (6). Since the analytical Hankel transform exists, we can also calculate the true result F_i at r_i.
4) Calculate the fitness (objective function) using

$$\Phi = \sqrt{\frac{\sum_{i=0}^{M-1}(\left|\frac{F(r_i)-F_i}{F_i}\right|)^2}{M}}, \tag{12}$$

where M is the total data points used to calculate the fitness (typically smaller than the total data points N). Since F_i can be very small (close to zero), we only consider F_i greater than a preset value.

III. NUMERICAL TEST

In this section, we use the particle swarm algorithm to calculate the optimal spacing and shift, and the matrix inversion method to calculate the filter coefficients based on analytical transform pairs for J_0 and J_1. Then the calculated filter is examined quantitatively based on analytical transform pairs. For comparison purpose, other filters are considered in this paper. These include the 801-point filter proposed by Anderson (called Anderson801 [21]), the 61-point filter by Guptasarma and Singh (called New61 only for J_0 [31]), the 241-point filters by Kong (Kong241 [29]), the 201-point filters used by Key (Key201 [28]), and the 201-point filters proposed by Werthmüller with careful multiple-time refinement (Wer201 [30]) and without refinement (called Brute-force201 [30]) The filter from our algorithm is referred as PSO201 in the paper. Finally, the obtained filter coefficients are applied to the Hankel transform calculation for the electromagnetic forward modeling to verify its effectiveness and practicability by comparing the result from our method with those from other filters. All the tests coded in Python run on a system of 4 processors with 12 GB RAM.

A. CALCULATION OF FILTER

Using the analytic transform function pair in (7) and (8), we design a 201-point filter (PSO201) based on a particle swarm algorithm. The number of individuals is 50 and the preset maximum number of iterations is 40. The Brute-force201 filter is calculated using the algorithm proposed by the work [30] and no refinement is applied [34]. The value of r considered ranges from 10^{-3} to 10^{7} m. The search ranges for the spacing and shifting are from 0 to 2 and -4 to 0, respectively. Preset value used in this paper for F_i is 10^{-20}.

For the Brute-force201 filter, the two dimensional spacing and shifting plane is uniformly discretized into 50 × 40 cells. If the relative difference of fitness between two consecutive iterations is less than 0.01 for more than 15 consecutive iterations, we consider to terminate the algorithm.

The convergence process of all particle for the particle swarm algorithm is shown in Fig. 2. As indicated in Fig. 2, at the beginning, the particle spreads the whole model space. As the algorithm proceeds, all particles converge rapidly to the optimal region.

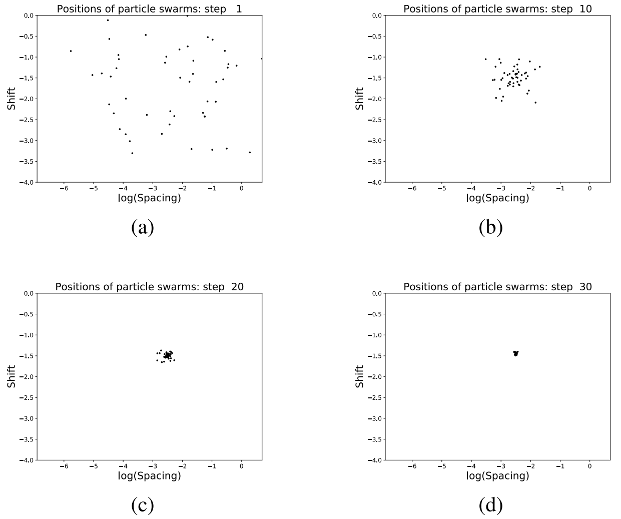

(a) (b)

(c) (d)

FIGURE 2. The positions of all particles at the (a) 1st, (b) 10th, (c) 20th and (d) 30th iterations during the optimization process of the particle swarm algorithm.

The convergence process for the spacing, shifting and minimum amplitude is shown in Fig. 3. It can be seen from Fig. 3 that as the optimization algorithm proceeds, the values of the group-best spacing, shift, and fitness converge fast at the beginning. After about 26 iterations, the group-best spacing and shift stay constantly as the iteration increases, indicating a convergence.

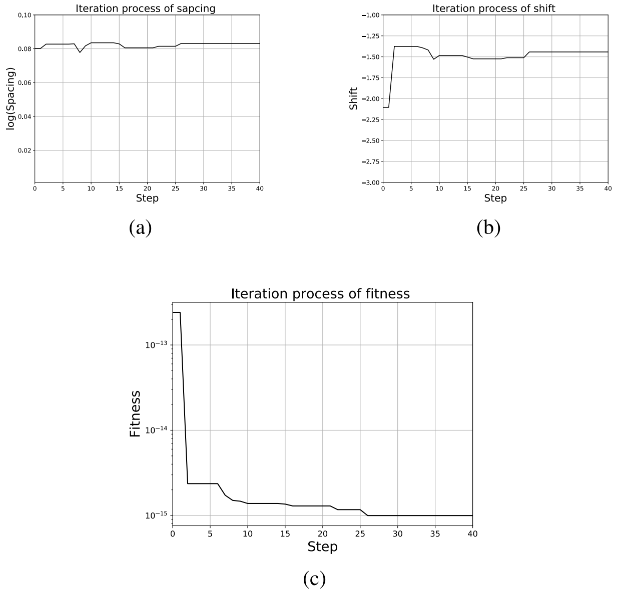

(a) (b)

(c)

FIGURE 3. The convergence process of the particle swarm algorithm for the (a) spacing, (b) shift and (c) fitness.

B. ANALYTICAL FUNCTION TEST

In this subsection, we carry out the quality test on the calculated PSO201 filters for J_0 and J_1 based on the analytic function pairs (7) and (8) from Anderson [19] and the following function pairs [31]:

$$\int_0^\infty lexp(-al)J_0(lr)dl = \frac{a}{(a^2+r^2)^{3/2}}, \tag{13}$$

$$\int_0^\infty lexp(-al)J_1(lr)dl = \frac{r}{(a^2+r^2)^{3/2}}, \tag{14}$$

where $a > 0$, $r > 0$.

We calculate (7) and (8) numerically using different filters mentioned above at different offset r. The comparison of relative errors from different filters for J_0 and j_1 is carried out in Fig. 4 and Fig. 5, respectively. As indicated in Fig. 4, for J_0 our calculated filter and Brute-force 201 have generally better accuracy over the whole considered range, followed by Wer201. In general, New61 performs worst among the considered filters. For J_1, our filter and Wer201 perform better than the rest. Key201 has a general poor performance over the considered range. As indicated in the figures, all the filters can be inaccurate outsider certain range (e.g., more than 10 in this example).

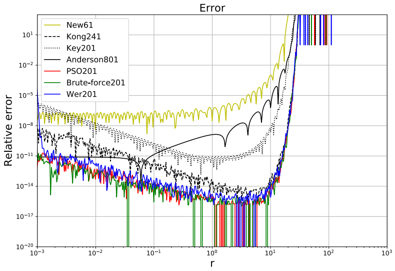

FIGURE 4. Relative errors of different digital filters of J_0 for the calculation of analytical function pair in (7).

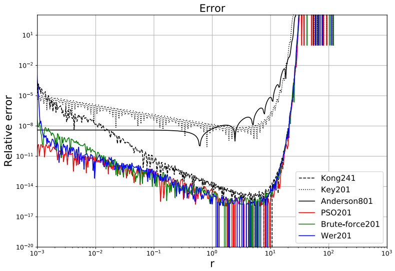

FIGURE 5. Relative errors of different digital filters of J_1 for the calculation of the analytical function pair in (8).

The comparison of relative errors from different filters for (13) is carried out in Fig. 6. In general, all the digital filters

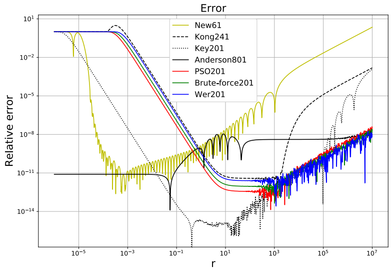

FIGURE 6. Relative errors of different digital filters of J_0 for the calculation of analytical function pair in (13).

have some certain ranges in which they can perform better than others. For example, the New61 filter performs better than Kong241, PSO201, Brute-force201 and Wer201 in the range (10^{-5} to 10^{-1}). Key201 is most accurate near $r = 1$. When r is larger than 10^3, PSO201, Brute-force201 and Wer201 perform better. Since PSO201, Brute-force201 and Wer201 is based on the same analytic function pair, they have generally similar numerical performance. As indicated in Fig. 6, since Anderson801 uses a longer filter, it is generally accurate over the whole considered range.

For J_1 filters, the comparison is shown in Fig. 7 for different offsets based on (14). As indicated in Fig. 7, Key201 is most accurate over a large range from less than 10^{-3} to larger than 10^3. The Anderson801 filter is accurate over the whole considered range with maximum relative errors of less than 10^{-8}. PSO201, Brute-force201 and Wer201 are more accurate at large offsets and relatively less accurate at short distances. Relative to all other considered filters, the Kong241 filter is generally less accurate.

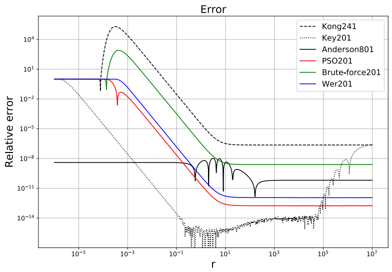

FIGURE 7. Relative errors of different digital filters of J_1 for the calculation of the analytical function pair in (14).

As indicated for both J_0 and J_1, the Anderson801 filter has better overall accuracy. However, it certainly needs more computing time compared with the other filters, which is also considered as an important factor for real applications. For large offsets typically encountered in real geophysical applications, the use of PSO201, Brute-force201 and Wer201 is desirable. Relative to Wer201, our filters are produced using a global optimizer without manual refinement steps (can be difficult even for a person with advanced expertise) and avoid potential local optima.

C. APPLICATION IN CSEM

To examine the practical application of the filter obtained with the particle swarm algorithm, three CSEM conductivity models in the work [30], are considered in this paper. The numerical performance of our PSO201 filter on these real applications is compared with the other filters considered in this paper.

Since these models do not have an analytical Hankel transform, we use the solution from the QWE algorithm proposed by key [28] as the reference result, based on which the relative difference for each filter is calculated. Because the QWE algorithm is considered accurate within around 15000 m, all the following comparisons are carried out at offsets less than 20000 m. Our algorithm is based on the direct matrix solution method of Kong [29] and Werthmüller *et al.* [30]. An open source code [34] is used to calculate EM responses for an electric dipole.

The first model is a marine CSEM two-layer model initially proposed by Kong [29], as indicated in Fig. 8. The resistivity of the ocean is 0.31 $\Omega \cdot$ m, and the uniform half-space is 1 $\Omega \cdot$ m. A x-directed horizontal electric dipole source with a frequency of 1 Hz is located in the sea at 50 m above the seafloor.

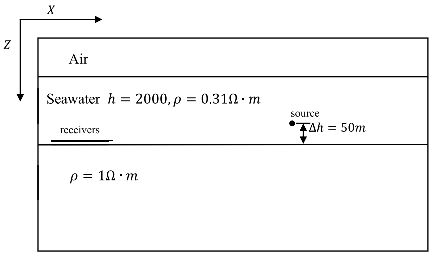

FIGURE 8. The two-layer CSEM model from Kong [29].

Fig. 9(a) shows the numerical performance for different filters based on the two-layer marine CSEM model. As indicated in the figure, PSO201, Brute-force201 and Wer201 have a similar numerical performance in terms of the minimal field magnitude calculated. They can accurately evaluate a field smaller than 10^{-25} V/m at an offset within larger than 15000 m. However, Key201 and And801 can only calculate a field larger than 10^{-22} V/m at a distance up to slightly larger than 10000 m. Kong241 is slightly better than Key201 and And801.

Fig. 9(b) shows the relative difference of the x-component electrical field for different filters using the QWE solution as

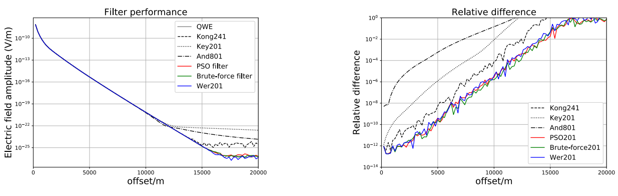

(a) (b)

FIGURE 9. The numerical performance comparison of different filters based on the half-space marine CSEM model from Kong [29]. (a) shows the calculated x-component electric field, and (b) shows the relative difference over a wide range against the QWE solution.

the reference. Quantitatively, it shows that PSO201, Brute-force201 and Wer201 produce the most accurate results with the smallest relative difference over the whole computational domain. Key201 performs much poorer than PSO201, Brute-force201 and Wer201. For this model, And801 performs poorest over the whole considered range especially at long offsets. It shows that for this model, the direct matrix inversion method can produce generally better filters. A comparison to the previous analytical cases indicates that the performance of a filter can be different for different problems.

The second model is a typical four-layer marine CSEM model used in Key [28] as shown in Fig. 10. The first layer is a 1000 m-deep seawater layer with resistivity of 0.30 $\Omega \cdot$ m. A 100 m-thick anomalous layer with resistivity of 100 $\Omega \cdot$ m is embedded in the 1 $\Omega \cdot$ m uniform half-space at 1000 m depth. The source is located at 10 m above the seafloor and the frequency used is 1 Hz. The receivers are located on the seafloor.

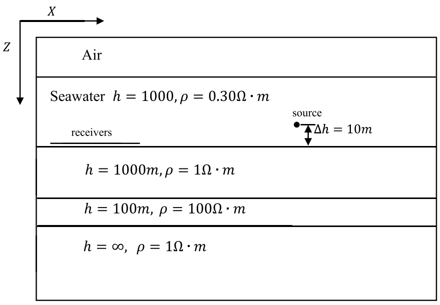
X
Z
Air
Seawater $h = 1000, \rho = 0.30\Omega \cdot m$
source
receivers
$\Delta h = 10m$
$h = 1000m, \rho = 1\Omega \cdot m$
$h = 100m,\ \rho = 100\Omega \cdot m$
$h = \infty,\ \rho = 1\Omega \cdot m$

FIGURE 10. **The four-layer marine CSEM model from Key (2012) [28].**

The comparison of the numerical performance in terms of maximum offset and minimal field magnitude evaluated by different filters is shown in Fig. 11(a). As indicated in the figure, for this model all the filters can calculate the field accurately within the range of [0, 20000] m. It clearly shows that the filters may provide a calculation at larger maximum offsets and with weaker signal. However, since QWE is considered accurate only within around 20000 m, it is unjustified to make a further comparison at an offset larger than 20000 m.

Fig. 11(b) shows the relative difference of the x-component electrical field for different filters based on the four-layer model. It shows that And801 and Kong241 perform poorest among all the considered filters. PSO201, Brute-force201 and Wer201 are more accurate than the rest over the whole computational range. Among the filters based on the matrix inversion method, Wer201 is most accurate for a large range. PSO201 performs better at small distances (e.g., less than 2500 m)

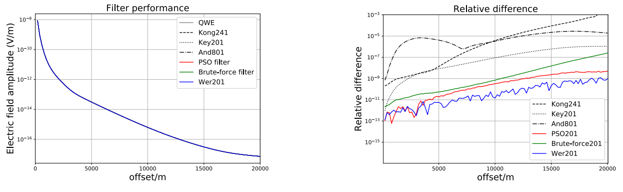

(a) (b)

FIGURE 11. **The numerical comparison of different filters based on the four-layer marine CSEM model [28]. (a) shows the calculated x-component electric field and (b) shows the relative difference over a wide range against the QWE solution.**

The third model considered is a three-layer land CSEM model as shown in Fig. 12 [30]. A 100 m-thick layer with resistivity of 500 $\Omega \cdot$ m is embedded at a depth of 1000 m in the 10 $\Omega \cdot$ m uniform half-space. The source operating at 1 Hz is located at 0.5 m depth, and the receiver depth is 0.8 m.

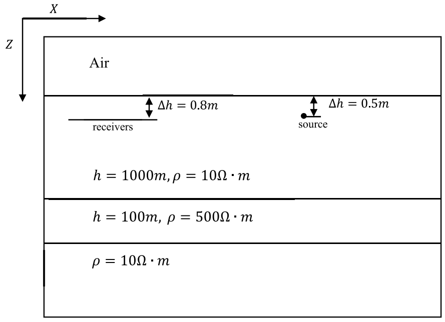
X
Z
Air
$\Delta h = 0.8m$
$\Delta h = 0.5m$
receivers
source
$h = 1000m, \rho = 10\Omega \cdot m$
$h = 100m,\ \rho = 500\Omega \cdot m$
$\rho = 10\Omega \cdot m$

FIGURE 12. **The land CSEM three-layer model [30].**

The x-component field is calculated over the range [0, 20000] m for different filters for the land three-layer model as shown in Fig. 13(a). Similar as in the previous case, all the filters have similar numerical performance within 20000 m in terms of minimum magnitude calculated. Within this range, all the filters produce comparable results for this model. A detailed relative difference comparison is shown in Fig. 13(b). For this case, Kong241 produces largest relative difference over the whole range. Brute-force, Key201 and And801 have a comparable accuracy. The filters based on the matrix inversion using optimal spacing and shift generally produce more accurate results.

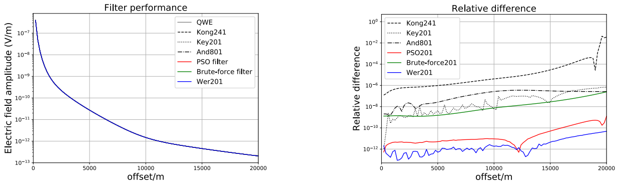

(a) (b)

FIGURE 13. **The numerical performance comparison of different filters based on the land 3-layer CSEM model [30]. (a) shows the calculated x-component electric field and (b) shows the relative difference over a wide range against the QWE solution.**

IV. CONCLUSION

The calculation of Hankel transforms based on the digital filter method needs to find the optimal spacing and shifting. This is commonly carried out using linear search algorithms on different grids (typically gradually refined and can potentially be trapped at local minima). In this paper we apply a particle swarm optimization algorithm to optimize the spacing and shift for the filter design (no refinement needed). This algorithm uses a group of particles and retains the best solution encountered during the search process. This algorithm can effectively avoid the use of gradual refinement process. The numerical performance of the calculated filter is compared with other published filters in terms of relative difference, and minimum field magnitude and maximum offsets calculated based on analytic function pairs and CSEM applications (i.e., two marine CSEM models and one land CSEM model).

For the analytic function pair, our algorithm is comparable with filters based on matrix inversion (Brute-force201 and Wer201). It performs much better at large offsets against the traditional filters (e.g., Anderson801, Kong241, Key201 and New61). For the two-layer marine model, our filter performs better than Anderson801, Kong241 and Key201 in terms of both relative difference, and minimum filed magnitude and maximum offsets calculated. Again, PSO201, Brute-force201 and Wer201 present a similar numerical performance. For the four-layer marine and three-layer land CSEM cases, all the considered filters have the similar minimum field magnitude and maximum offsets over the considered offset range. The relative difference for PSO201, Brute-force201 and Wer201 is generally comparable (PSO201 is slightly larger than Wer201 and smaller than Brute-force201) and much smaller than Anderson801, Kong241 and Key201. However, the Wer201 filter is based on the spacing and shift parameters generated with gradual refinement steps and the choice can be subjective due to their random distribution in the solution space [30]. It is worth noting that although we use the particle swarm optimization algorithm to optimise the spacing and shifting of a digital filter in this paper, other similar methods, such as monarch butterfly optimization (MBO), earthworm optimization algorithm (EWA), elephant herding optimization (EHO), moth search (MS) algorithm, Slime mould algorithm (SMA) and Harris hawks optimization (HHO), can be also applied equally for this purpose.

REFERENCES

[1] D. Yang and D. W. Oldenburg, "Three-dimensional inversion of airborne time-domain electromagnetic data with applications to a porphyry deposit," *Geophysics*, vol. 77, no. 2, pp. B23–B34, Mar. 2012.

[2] C. Yin, X. Huang, Y. Liu, and J. Cai, "Footprint for frequency-domain airborne electromagnetic systems," *Geophysics*, vol. 79, no. 6, pp. E243–E254, Nov. 2014.

[3] R. Liu, R. Guo, J. Liu, and G. Ma, "A hybrid solver based on IEM and vector FEM for 3D CSEM modelling," *Geophysics*, vol. 83, no. 5, pp. 1–42, 2018.

[4] R. Liu, J. Liu, J. Wang, Z. Liu, and R. Guo, "1D electromagnetic response modeling with arbitrary source-receiver geometry based on vector potential and its implementation in MATLAB," *Geophysics*, vol. 85, no. 3, pp. F27–F38, May 2020.

[5] W. Tang, Y. Li, A. Swidinsky, and J. Liu, "Three-dimensional controlled-source electromagnetic modelling with a well casing as a grounded source: A hybrid method of moments and finite element scheme," *Geophys. Prospecting*, vol. 63, no. 6, pp. 1491–1507, Nov. 2015.

[6] H. Cai, X. Hu, J. Li, M. Endo, and B. Xiong, "Parallelized 3D CSEM modeling using edge-based finite element with total field formulation and unstructured mesh," *Comput. Geosci.*, vol. 99, pp. 125–134, Feb. 2017.

[7] J. Li, C. G. Farquharson, and X. Hu, "3D vector finite-element electromagnetic forward modeling for large loop sources using a total-field algorithm and unstructured tetrahedral grids," *Geophysics*, vol. 82, no. 1, pp. E1–E16, Jan. 2017.

[8] G. Li, S. Duan, H. Cai, B. Han, and Y. Ye, "An improved interpolation scheme at receiver positions for 2.5 D frequency-domain marine controlled-source electromagnetic forward modelling," *Geophys. Prospecting*, vol. 68, no. 5, pp. 1657–1675, 2020.

[9] J. Li, R. Liu, R. Guo, Y. Wang, and X. Wang, "3D finite difference modeling of controlled-source electromagnetic response in frequency domain based on a modified curl-curl equation," *J. Appl. Geophys.*, vol. 183, Dec. 2020, Art. no. 104202.

[10] I. Longman, "Tables for the rapid and accurate numerical evaluation of certain infinite integrals involving bessel functions," *Math. Tables Other Aids to Comput.*, vol. 11, no. 59, pp. 166–180, 1957.

[11] R. Piessens, "Gaussian quadrature formulae for integrals involving bessel functions," *Math. Comput.*, vol. 26, no. 120, p. 1016, Oct. 1972.

[12] B. W. Suter, "Fast nth-order hankel transform algorithm," *IEEE Trans. Signal Process.*, vol. 39, no. 2, pp. 532–536, Aug. 1991.

[13] A. V. Oppenheim, G. V. Frisk, and D. R. Martinez, "Computation of the hankel transform using projections," *J. Acoust. Soc. Amer.*, vol. 68, no. 2, pp. 523–529, Aug. 1980.

[14] S. Candel, "Dual algorithms for fast calculation of the Fourier-bessel transform," *IEEE Trans. Acoust., Speech, Signal Process.*, vol. 29, no. 5, pp. 963–972, Oct. 1981.

[15] S. W. Rowland, "Computer implementation of image reconstruction formulas," in *Image Reconstruction From Projections: Implementation and Applications*, vol. 32, G. T. Herman, Ed. Berlin, Germany: Springer-Verlag, 1979, pp. 9–70, doi: 10.1007/3-540-09417-2_2.

[16] D. P. Ghosh, "The application of linear filter theory to the direct interpretation of geoelectrical resistivity sounding measurements," *Geophys. Prospecting*, vol. 19, no. 2, pp. 192–217, Jun. 1971.

[17] O. Koefoed, "A note on the linear filter method of interpreting resistivity sounding data," *Geophys. Prospecting*, vol. 20, no. 2, pp. 403–405, Jun. 1972.

[18] O. Koefoed and F. J. H. Dirks, "Determination of resistivity sounding filters by the wiener-hopf least-squares method," *Geophys. Prospecting*, vol. 27, no. 1, pp. 245–250, Mar. 1979.

[19] W. L. Anderson, "Improved digital filters for evaluating Fourier and hankeltransform integrals," US Geological Surv., Tech. Rep. USGS-GD-75-012, 1975.

[20] W. L. Anderson, "Numerical integration of related hankel transforms of orders 0 and 1 by adaptive digital filtering," *Geophysics*, vol. 44, no. 7, pp. 1287–1305, Jul. 1979.

[21] W. L. Anderson, "Fast hankel transforms using related and lagged convolutions," *ACM Trans. Math. Softw.*, vol. 8, no. 4, pp. 344–368, Dec. 1982.

[22] W. L. Anderson, "A hybrid fast hankel transform algorithm for electromagnetic modeling," *Geophysics*, vol. 54, no. 2, pp. 263–266, Feb. 1989.

[23] H. K. Johansen and K. Sørensen, "Fast Hankel transforms," *Geophys. Prospecting*, vol. 27, no. 4, pp. 876–901, Dec. 1979.

[24] M. Bichara and J. Lakshmanan, "Fast automatic processing of resistivity soundings," *Geophys. Prospecting*, vol. 24, no. 2, pp. 354–370, Jun. 1976.

[25] M. Bernabini and E. Cardarelli, "The use of filtered bessel functions in direct interpretation of geoelectrical soundings," *Geophys. Prospecting*, vol. 26, no. 4, pp. 841–852, 1978.

[26] A. D. Chave, "Numerical integration of related hankel transforms by quadrature and continued fraction expansion," *Geophysics*, vol. 48, no. 12, pp. 1671–1686, Dec. 1983.

[27] K. Key, "1D inversion of multicomponent, multifrequency marine CSEM data: Methodology and synthetic studies for resolving thin resistive layers," *Geophysics*, vol. 74, no. 2, pp. F9–F20, Mar. 2009.

[28] K. Key, "Is the fast hankel transform faster than quadrature?" *Geophysics*, vol. 77, no. 3, pp. F21–F30, May 2012.

[29] F. N. Kong, "Hankel transform filters for dipole antenna radiation in a conductive medium," *Geophys. Prospecting*, vol. 55, no. 1, pp. 83–89, Jan. 2007.

[30] D. Werthmüller, K. Key, and E. C. Slob, "A tool for designing digital filters for the hankel and Fourier transforms in potential, diffusive, and wavefield modeling," *Geophysics*, vol. 84, no. 2, pp. F47–F56, Mar. 2019.

[31] D. Guptasarma and B. Singh, "New digital linear filters for Hankel J0 and J1 transforms [link]," *Geophys. Prospecting*, vol. 45, no. 5, pp. 745–762, 2003.

[32] R. Eberhart and J. Kennedy, "A new optimizer using particle swarm theory," in *Proc. MHS95. Proc. 6th Int. Symp. Micro Mach. Human Sci.*, Oct. 1995, pp. 39–43.

[33] Y. Shi and R. C. Eberhart, "Empirical study of particle swarm optimization," in *Proc. Congr. Evol. Computation*, Jul. 1999, pp. 1945–1950.

[34] D. Werthmüller, "An open-source full 3D electromagnetic modeler for 1D VTI media in Python: Empymod," *Geophysics*, vol. 82, no. 6, pp. WB9–WB19, Nov. 2017.

LIANG ZENG is currently pursuing the Ph.D. degree in mathematics with the School of Mathematical Sciences, Xiamen University, Xiamen, China.

His research interests include developing efficient optimization algorithms and image processing.

JINTAI LI was born in 1998. He received the B.S. degree in geophysics from Central South University, Changsha, China, in 2020, where he is currently pursuing the M.S. degree.

JIANXIN LIU received the Ph.D. degree from Central South University, Changsha, China, in 2006.

He is currently a Professor with the School of Geosciences and Info-Physics, Central South University. His research interests include geophysical data processing and interpretation, application of geophysics in mineral exploration, and geophysical forward modeling and inversion.

RONGWEN GUO received the Ph.D. degree from Central South University, Changsha, China, in 2011.

He is currently a Professor with the School of Geosciences and Info-Physics, Central South University. His research interests include data processing forward modeling and inversion of geophysical data, especially for electromagnetic method and geophysical data uncertainty estimation.

HANG CHEN was born in 1998. He received the B.S. degree in geophysics from Central South University, Changsha, China, in 2020.

RONG LIU is currently pursuing the Ph.D. degree in geophysics with the School of Geosciences and Info-Physics, Central South University, Changsha, China.

His research interest includes three-dimensional EM fast forward modeling in geophysics.